

Bifurcation of spiking oscillations from a center in resonate-and-fire neurons

Oleg Makarenkov^{1*†}, Marianne Bezaire^{2†} and Michael Hasselmo^{2†}

¹Department of Mathematical Sciences, The University of Texas at Dallas, 800 West Campbell Road, Richardson, 75080, Texas, United States.

²Kilichand Center for Integrated Life Sciences and Engineering, Boston University, 610 Commonwealth Ave, Boston, 02215, Massachusetts, United States.

*Corresponding author(s). E-mail(s): makarenkov@utdallas.edu;
Contributing authors: mbezaire@bu.edu; hasselmo@gmail.com;

†These authors contributed equally to this work.

Abstract

The theta rhythm is important for many cognitive functions including spatial processing, memory encoding, and memory recall. The information processing underlying these functions is thought to rely on consistent, phase-specific spiking throughout a theta oscillation that may fluctuate significantly in baseline (center of oscillations), frequency, or amplitude. Experimental evidence shows that spikes can occur at specific phases even when the baseline membrane potential varies significantly, such that the integrity of phase-locking persists across a large variability in spike threshold. The mechanism of this precise spike timing during the theta rhythm is not yet known and previous mathematical models have not reflected the large variability in threshold potential seen experimentally. Here we introduce a straightforward mathematical neural model capable of demonstrating a phase-locked spiking in the face of significant baseline membrane potential fluctuation during theta rhythm. This novel approach incorporates a degenerate grazing bifurcation of an asymptotically stable oscillation. This model suggests a potential mechanism for how biological neurons can consistently produce spikes near the peak of a variable membrane potential oscillation.

Keywords: theta rhythm, nonsmooth dynamical system, degenerate grazing bifurcation, spike threshold, mathematical modeling

1 Introduction

Experimental data indicates that the theta rhythm in hippocampus and associated cortical structures plays an important role in memory function. For example, the efficacy of memory encoding in behavioral tasks correlates with the magnitude of hippocampal theta rhythm (Berry and Thompson 1978; Winson 1978; Givens and Olton 1990). The theta rhythm, commonly

observed as an oscillation in the local field potential, is also visible in individual neuron activity. The spiking of hippocampal neurons in extracellular recordings shows strong dependence on the phase of hippocampal theta rhythm (Fox et al. 1986; Buzsáki et al. 1983), and theta rhythmicity is commonly observed in the spiking autocorrelograms of hippocampal (O’Keefe and Recce 1993) and entorhinal neurons (Hafting et al. 2008).

Intracellular recording of hippocampal neurons reveals prominent theta rhythm oscillations of the membrane potential during observation of theta rhythm in the extracellular field potential (Fujita and Sato 1964; Leung and Yim 1986; Kamondi et al. 1998; Harvey et al. 2009). Comparison of spike times relative to both intracellular membrane potential and local field potential recordings reveal a consistent phase preference of the timing of spikes relative to the intracellular membrane potential. The spiking activity occurs on the rising phase near the peak of each cycle in hippocampal intracellular recordings by Harvey et al. (2009) and Kamondi et al. (1998) as well as in observations in entorhinal cortex by Schmidt-Hieber and Häusser (2013). The phase preference is also apparent in the entorhinal recordings of Domnisoru et al. (2013), where the intracellular spike phase preference persists across large variations in theta amplitude and baseline voltage (see Fig. 1). The variations in amplitude and baseline of the theta oscillation are sufficient for the intracellular theta rhythm of the cell to reach membrane potentials within the range of the spike threshold prior to peaking; however, the threshold appears dynamic and able to bias the cell to spike towards the peak of the intracellular rhythm even when the peak potential is relatively depolarized compared to other cycles of the rhythm. The ability of spike phase preference to remain consistent across a range of theta cycle amplitudes has not been widely explored in computational models, although there is robust experimental evidence of the concomitant spike threshold variability (Higgs and Spain 2011; Platkiewicz and Brette 2011; Tsuno et al. 2013; Wester and Contreras 2013; Fontaine et al. 2014) and functional benefits of spike threshold variability have been modeled (Itskov et al. 2011; Huang et al. 2016).

Many neurons show theta phase precession relative to the theta rhythm in the field potential (O'Keefe and Recce 1993; Skaggs et al. 1996; Huxter et al. 2003; Fernández-Ruiz et al. 2017), which could be interpreted as instability of firing phase. However, the studies cited above specifically show that spiking maintains phase relationships to intracellular membrane potential, while both spiking and intracellular membrane potential shift in phase relative to the field potential oscillations (Harvey et al. 2009; Domnisoru et al.

2013; Schmidt-Hieber and Häusser 2013). Models of oscillatory interference can produce spikes phase-locked to the peak of the intracellular theta oscillation (Bush and Burgess 2014), although they generally assume a constant theta baseline and stable amplitude. Notably, a continuous attractor network model also produced spikes that were phase-locked to the intracellular theta peak when combined with an oscillatory interference model, but not when combined with a slow, depolarizing ramp (Schmidt-Hieber and Häusser 2013). Other models start from an assumption of phase-locked spiking to study other phenomena rather than examining the factors causing the phase-locked spikes (O'Keefe and Recce 1993; Lengyel et al. 2003; O'Keefe and Burgess 2005).

In the present paper we use a planar neural model of Izhikevich (2001) to demonstrate mathematically how simple intrinsic dynamics within a neuron or in local circuits of neurons can maintain a phase-locked intracellular spike preference robust to changes in theta amplitude. The novelty of our approach is that it not only predicts a range of parameters where the response of Izhikevich's model is phase-locked (with 1 spike per oscillation), but also generates spikes on the crest of a wave, rather than appearing on the rising phase of a wave, resembling some typical aspects of the dynamics of Fig. 1 of Domnisoru et al. (2013).

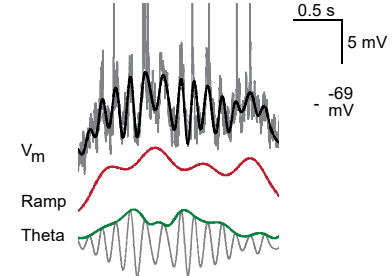


Fig. 1 Experimental observations of grid cell activity, adapted from Domnisoru et al. (2013). The top trace shows the intracellular membrane potential (with truncated spikes) in gray. The red trace below shows the fluctuation in the baseline potential, while the variations in frequency and amplitude of the theta oscillation are apparent in the theta component shown at the bottom (with envelope in green). The sum of the ramp and theta components is shown in black overlay at top. The flexibility in spike threshold to enable spiking that is phase-locked to the peak is clear at the positions marked with black annotations. Figure adapted and reprinted by permission from Nature Publishing Group.

Our mathematical analysis is based on bifurcation theory. We introduce a small parameter $\varepsilon \geq 0$ in such a way that the model admits a family of cycles for $\varepsilon = 0$ and one of the cycles just touches the firing threshold. Such a cycle is known as grazing cycle in nonsmooth bifurcation theory, see (DiBernardo et al. 2008) and (Makarenkov and Lamb 2012). The configuration where the grazing cycle is embedded into a family of cycles is called *degenerate* because it can be destroyed by small perturbation. It has been already noticed in the literature that the degenerate grazing cycle in impulsive systems is capable to create asymptotic stability under certain types of perturbations, see (Zhao and Dankowicz 2006; Yagasaki 2004; Turaev and Rom-Kedar 1998). In the present paper we use a degenerate grazing cycle to prove the occurrence (termed *grazing bifurcation*) of asymptotically stable spiking oscillations in a simple neuron model. Various dynamics of spiking neuron models resulting from grazing bifurcations has been discussed in (Coombes et al. 2012; Nicola and Campbell 2016), but grazing bifurcation of asymptotically stable oscillations hasn't been addressed in the earlier literature. To catch the required phenomenon we establish a new theorem about bifurcation of stable periodic solutions from a grazing cycle in impulsive systems, which might be of independent interest in nonsmooth bifurcation theory.

2 Methods

We used Izhikevich's resonate-and-fire neuron model (Izhikevich (2001, 2007)) to prove the existence of an asymptotically stable spiking cycle with some key differences. As in Izhikevich's model, our reset condition is triggered by the voltage trajectory crossing a defined threshold. However, the reset condition in Izhikevich's resonate-and-fire model acts as $h \rightarrow 0$, while we consider $h \rightarrow h + \Delta h$ in our analysis. The later impact condition allows us to have a controllable estimate of the magnitude of the impact that we use in our perturbation approach. Reset conditions different from the one in Izhikevich (2001, 2007) in relation to resonate-and-fire neuron model have been also considered in e.g. Mukhopadhyay (2010) and Marangio et al. (2019).

The second key difference is that unlike most of the methods in neuroscience (see e.g. Izhikevich (2007)) that use global information, such as unstable focus (akin to producing spontaneous intracellular activity in a neuron), or Hopf bifurcation, to generate cyclic spiking behavior, our method is based on a novel *grazing bifurcation* and uses local information near one particular trajectory (of the associated unperturbed model) touching the reset threshold. For the parameters that we consider for the most of the paper, the model under consideration does indeed have an unstable focus, but we also give an example of parameters (Section 3.1.1) where our perturbation approach produces spiking oscillations that surround an asymptotically stable focus. Our theorem provides formulas as for how the reset condition in the former case should be different from reset condition in the later case for asymptotically stable spiking oscillations to exist in both cases. All numerical simulations were conducted using Mathematica 12.1.

2.1 An orbitally stable nearly grazing limit cycle

First, we determined the conditions for the existence of an orbitally stable nearly grazing limit cycle in a non-linear system with resets. Starting from a set of model equations for a resonate-and-fire model of (Izhikevich 2007, §8.1.2-§8.1.4) (see also Hasselmo and Shay (2014)), we incorporated a small parameter ε that destroys the center phase portrait, as shown in equation (1).

$$\begin{aligned} \dot{v} &= \varepsilon m_1 v + k_1 h + \varepsilon m v^2, \\ \dot{h} &= k_2 v + \varepsilon m_2 h, \end{aligned} \quad (1)$$

$$\begin{aligned} v(t) &\rightarrow v(t) + \varepsilon \bar{v}, \\ h(t) &\rightarrow h(t) + \sqrt{\varepsilon} \cdot \bar{h}, \end{aligned} \quad \text{if } v(t) = v_{th}, \quad (2)$$

In equations (1)-(2), v represents the membrane potential of the model neuron in arbitrary units, t represents the time in arbitrary units, and h represents the activation of a hyperpolarization-activated cation channel in arbitrary units. The parameters m, m_1, m_2, \bar{v} can be of arbitrary signs including zeros, while parameters $k_1, k_2, \bar{h}, v_{th}$ have to satisfy

$$k_1 > 0, \quad k_2 < 0, \quad v_{th} > 0, \quad \bar{h} \neq 0, \quad 0 < \varepsilon \ll 1. \quad (3)$$

Note that these constraints correspond to biological properties of the h current. The positive value of $k_1 > 0$, represents the fact that the h current is a cation current, and the negative value of $k_2 < 0$, represents the fact that the h current is a hyperpolarization activated current that is more activated when v reaches more hyperpolarized (negative) values. The threshold v_{th} must have a positive value corresponding to a quiescent state of the neuron at resting potential.

The parameters v_{th} , \bar{v} , and \bar{h} define the reset rule. This system produces a discontinuous limit cycle shown in Figure 2 (right).

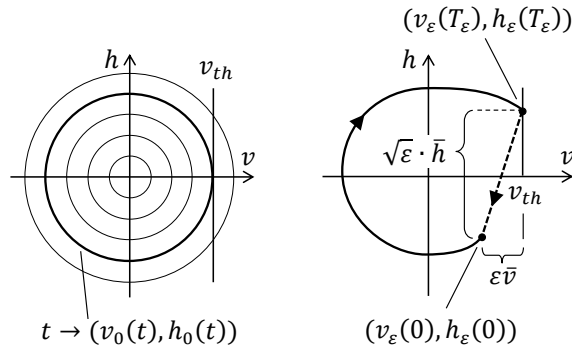


Fig. 2 Left: Trajectories of system (4). Right: Discontinuous limit cycle of system (1)-(2) with one impact per period that this paper intends to establish.

Along with system of equations (1)-(2), consider the reduced system where $\varepsilon = 0$, that gives

$$\begin{aligned}\dot{v} &= k_1 h, \\ \dot{h} &= k_2 v.\end{aligned}\tag{4}$$

Equilibrium $(v, h) = 0$ of equation (4) is of center type and solutions of equation (4) form a family cycles of period $T_0 = 2\pi/\sqrt{-k_1 k_2}$, see Fig. 2 left. Each such cycle is Lyapunov stable, but not asymptotically stable. In what follows, we prove that when ε changes from $\varepsilon = 0$ to small $\varepsilon > 0$ the family of cycles disappears except for the cycle that crosses $v = v_{th}$ transversely (bold cycle in Fig. 2 left). The grazing cycle persists and transforms to an asymptotically stable discontinuous limit cycle of (1)-(2) as ε crosses 0 (Fig. 2 right). Such a transformation of dynamic behavior (from a Lyapunov stable family of cycles to an asymptotically stable isolated cycle) is usually referred to as

bifurcation in the literature, see e.g. (Christopher et al. 2024, Chapter II, Definition 2.3).

To prove persistence of the grazing cycle as ε crosses 0, we show that the cross-section $v = v_{th}$ induces a Poincaré map $h \mapsto P_\varepsilon(h)$ of system (1)-(2). All points of $(-\infty, 0]$ are fixed points for P_0 . Using the Taylor expansion of $h \mapsto P_\varepsilon(h)$ near $(h, \varepsilon) = (0, 0)$, we prove that the fixed point $h = 0$ of P_0 transforms to an asymptotically stable fixed point h_ε of P_ε , i.e. $h_\varepsilon \rightarrow 0$ as $\varepsilon \rightarrow 0$. Moreover, we provide a formula for the limit, as $\varepsilon \rightarrow 0$ of the characteristic multiplier $\rho_\varepsilon = (P_\varepsilon)'(h_\varepsilon)$ of the discontinuous limit cycle corresponding to the fixed point h_ε . Remarkably, the limit of ρ_ε is different from 1 even though the characteristic multiplier of any cycle of reduced system (4) is 1, which discontinuity in the behavior of ρ_ε is typical for grazing bifurcations.

The central role in our analysis is played by the following constants a_0 and b_0 :

$$a_0 = \frac{1}{k_2 v_{th}}, \quad b_0 = 2 \frac{\pi(m_1 + m_2)}{\sqrt{-k_1 k_2}} v_{th} + \bar{v}, \tag{5}$$

which are defined if condition (3) holds. The core of our method is the following theorem.

Theorem 1 Assume that system (4) is of center type, i.e. (3) holds. Denote by $t \mapsto (v_0(t), h_0(t))$ the cycle of (4) that touches the line $v = v_{th} > 0$ (bold cycle in Fig. 2 left). If

$$\bar{h} \neq 0, \quad b_0 < 0, \tag{6}$$

$$\frac{\bar{h}^2 + b_0/a_0^2}{2\bar{h}} + \bar{h} < 0, \tag{7}$$

then, for each $\varepsilon > 0$ sufficiently small, the system (1)-(2) admits an asymptotically stable T_ε -periodic limit cycle $t \mapsto (v_\varepsilon(t), h_\varepsilon(t))$ of one impact per period and satisfying

$(v_\varepsilon(t), h_\varepsilon(t)) \rightarrow (v_0(t), h_0(t))$, $T_\varepsilon \rightarrow T_0$, as $\varepsilon \rightarrow 0$, where T_0 is the minimal period of the cycle (v_0, h_0) . The characteristic multiplier ρ_ε of the limit cycle $(v_\varepsilon, h_\varepsilon)$ satisfies

$$\lim_{\varepsilon \rightarrow 0} \rho_\varepsilon = \rho_0, \quad \text{where } \rho_0 = \frac{\bar{h}^2 + b_0/a_0^2}{|\bar{h}^2 - b_0/a_0^2|} \text{sign}(\bar{h}). \tag{8}$$

We note that condition (6) ensures that $\rho_0 \in (-1, 1)$.

Throughout the paper, same notation $I(\cdot)$ stays for various (different) functions whose explicit formula is not used in proofs (and doesn't influence conclusions).

We remind the reader that, for a scalar function of 3 variables $(t, h, \varepsilon) \mapsto f(t, h, \varepsilon)$, the Taylor Theorem for power series of order 2 about $(t, h, \varepsilon) = 0$ reads as, see e.g. (Lang 1993, Ch. XIII, §6),

$$f(y) = f(0) + Df(0)y + \frac{D^2f(0)}{2}y^2 + \frac{D^3f(y_*)}{6}y^3,$$

where

$$y = \begin{pmatrix} t \\ h \\ \varepsilon \end{pmatrix}, \quad y_* = \begin{pmatrix} t_* \\ h_* \\ \varepsilon_* \end{pmatrix},$$

and y^2 is 2-tuple (y, y) , y^3 is 3-tuple (y, y, y) , Df, D^2f, D^3f are first, second, and third Fréchet derivatives of f with respect to the vector (t, h, ε) . The term D^2f is called Hessian or tensor of order 2, and D^3f is tensor of order 3. The space of 2-tuples of vectors of \mathbb{R}^3 is denoted $R^{3 \times 3}$ and the space of 3-tuples of vectors of \mathbb{R}^3 is denoted $\mathbb{R}^{3 \times 3 \times 3}$.

Lemma 1 Let, for every $(t, h, \varepsilon) \in \mathbb{R}^3$, the function

$$I(t, h, \varepsilon) : \mathbb{R}^{3 \times 3 \times 3} \rightarrow \mathbb{R}$$

be a tensor of order 3, that is C^2 smooth with respect to the variables t, h, ε . Consider the equation

$$t^2 + ath + b\varepsilon + ct\varepsilon + ph\varepsilon + q\varepsilon^2 + I(t, h, \varepsilon) \begin{pmatrix} t \\ h \\ \varepsilon \end{pmatrix}^3 = 0, \quad (9)$$

where $a, b, c, p, h, q \in \mathbb{R}$ are arbitrary constants. Then, given $\gamma > 0$ there exists $\delta > 0$ such that for any $h, \varepsilon \neq 0$ that satisfy

$$\sqrt{h^4 + \varepsilon^2} \leq \delta \quad \text{and} \quad \frac{(ah)^2 - 4b\varepsilon}{\sqrt{h^4 + \varepsilon^2}} \geq \gamma \quad (10)$$

the equation (9) admits exactly two solutions t . The least of the two solutions is given by

$$t = \frac{1}{2} \left(-ah - \sqrt{(ah)^2 - 4b\varepsilon} \right) + I(h, \varepsilon) \sqrt{h^4 + \varepsilon^2},$$

where I is C^1 in $\sqrt{h^4 + \varepsilon^2} \leq \delta$.

Even though the requirement of $\varepsilon > 0$ is needed for Theorem 1, the proof of Lemma 1 works for any $\varepsilon \neq 0$, so we didn't restrict the sign of ε in the formulation of Lemma 1.

To formulate the next lemma we denote by $t \mapsto (V, H)(t, v_0, h_0, \varepsilon)$ the solution $t \mapsto (v, h)(t)$ of system (1) with the initial condition $(v, h)(0) = (v_0, h_0)$.

In what follows, for functions of several variables, a letter in subscript refers to partial derivative with the respect to the corresponding variable, for example V_h is partial derivative of V with respect to h and V_{vh} is mixed partial derivative of V with respect to v and h . For functions of one variable, a letter in subscript refers to parameter, i.e. a function $P_\varepsilon : \mathbb{R} \rightarrow \mathbb{R}$ is an ε -dependent function and $(P_\varepsilon)'$ is the derivative of such a function.

When it doesn't cause confusion, vectors rows are identified with vectors columns. For example, in Lemma 2 below the 4-dimensional vector $x_0 = (T, v, h, \varepsilon)$ stays for $(T, v, h, \varepsilon)^T$.

Lemma 2 Let $T_0 > 0$ be the minimal period of the cycle $(v_0(t), h_0(t))$ as defined in Theorem 1. With the notation $x_0 = (T_0, v_{th}, 0, 0)$, it holds

$$\begin{pmatrix} V_v(x_0) & V_h(x_0) \\ H_v(x_0) & H_h(x_0) \\ V_\varepsilon(x_0) \\ H_\varepsilon(x_0) \end{pmatrix} = \begin{pmatrix} 1 & 0 \\ 0 & 1 \\ \pi(m_1 + m_2) \\ 0 \end{pmatrix}, \quad \omega = \sqrt{-k_1 k_2},$$

$$\begin{aligned} V_t(x_0) &= 0, & H_t(x_0) &= k_2 v_{th}, & a_0 H_t(x_0) &= 1, \\ V_{vv}(x_0) &= V_{vh}(x_0) = V_{hh}(x_0) = H_{vv}(x_0) = \\ &= H_{vh}(x_0) = H_{hh}(x_0) = 0, \\ V_{th}(x_0) &= k_1, & V_{tt}(x_0) &= k_1 k_2 v_{th}. \end{aligned}$$

Proof of Theorem 1. Step 1: *Computing the expansion of the time map $T(h, \varepsilon)$.* Expanding $(T, h, \varepsilon) \rightarrow V(T, v_{th} + \varepsilon \bar{v}, h, \varepsilon)$ in Taylor series about $(T, h, \varepsilon) = (T_0, 0, 0)$ and denoting $x_0 = (T_0, v_{th}, 0, 0)$ one has the following equation for time map $T(h, \varepsilon)$:

$$\begin{aligned} 0 &= -v_{th} + V(T, v_{th} + \varepsilon \bar{v}, h, \varepsilon) = \\ &= -v_{th} + v_{th} + V_t(x_0)(T - T_0) + \\ &\quad + V_h(x_0)h + V_v(x_0)\bar{v}\varepsilon + V_\varepsilon(x_0)\varepsilon + \\ &\quad + \frac{1}{2}V_{tt}(x_0)(T - T_0)^2 + V_{th}(x_0)(T - T_0)h + \\ &\quad + V_{t\varepsilon}(x_0)(T - T_0)\varepsilon + V_{tv}(x_0)(T - T_0)\bar{v}\varepsilon + \\ &\quad + \frac{1}{2}V_{hh}(x_0)h^2 + V_{h\varepsilon}(x_0)h\varepsilon + \frac{1}{2}V_{\varepsilon\varepsilon}(x_0)\varepsilon^2 + \\ &\quad + I(T, h, \varepsilon) ((T - T_0, h, \varepsilon)^T)^3. \end{aligned}$$

Using Lemma 2 to delete zero terms and applying Lemma 1 (with $a = a_0$ and $b = b_0$) to solve for T , we get

$$T(h, \varepsilon) = T_0 - a_0 h - \sqrt{(a_0 h)^2 - b_0 \varepsilon} + I(h, \varepsilon) \sqrt{h^4 + \varepsilon^2}, \quad (11)$$

where

$$a_0 = \frac{V_{th}(x_0)}{V_{tt}(x_0)}, \quad b_0 = \frac{2(V_\varepsilon(x_0) + V_v(x_0)\bar{v})}{V_{tt}(x_0)}.$$

Condition (10) of Lemma 1 will be verified later.

Step 2: *Expanding the Poincaré map $P_\varepsilon(h) = H(T(h, \varepsilon), v_{th} + \varepsilon\bar{v}, h, \varepsilon) + \sqrt{\varepsilon} \cdot \bar{h}$ in powers of (h, ε) . Since*

$$H(T, v_{th} + \varepsilon\bar{v}, h, \varepsilon) = H_t(x_0)(T - T_0) + H_h(x_0)h + (H_\varepsilon(x_0) + H_v(x_0)\bar{v})\varepsilon + I(T, h, \varepsilon)((T - T_0, h, \varepsilon)^T)^2,$$

we use (11) to get

$$P_\varepsilon(h) = \bar{P}_\varepsilon(h) + o(h, \varepsilon), \quad o(h, \varepsilon) = I(h, \varepsilon) \left((\sqrt{h^4 + \varepsilon^2}, h, \varepsilon)^T \right)^2, \quad (12)$$

where

$$\bar{P}_\varepsilon(h) = -H_t(x_0)a_0h - H_t(x_0)\sqrt{(a_0h)^2 - b_0\varepsilon} + h + \sqrt{\varepsilon} \cdot \bar{h}.$$

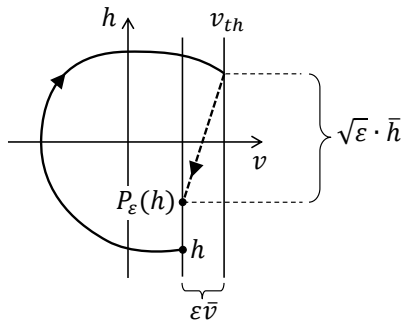


Fig. 3 Poincaré map of system (1)-(2) induced by cross-section $v = v_{th} + \varepsilon\bar{v}$.

Step 3: *Studying the dynamics of the reduced map $\bar{P}_\varepsilon(h)$. Solving $\bar{P}_\varepsilon(h) = h$, one gets $\bar{h}_\varepsilon =$*

$\frac{\bar{h}^2 + H_t(x_0))^2 b_0}{2H_t(x_0)a_0\bar{h}}\sqrt{\varepsilon}$, which can be simplified as

$$\bar{h}_\varepsilon = \frac{\bar{h}^2 + H_t(x_0)^2 b_0}{2\bar{h}}\sqrt{\varepsilon}, \quad (13)$$

as $H_t(x_0)a_0 = 1$ according to formulas of Lemma 2 and formula (5). Using same formulas, computation of $(\bar{P}_\varepsilon)'(\bar{h}_\varepsilon)$ yields

$$(\bar{P}_\varepsilon)'(\bar{h}_\varepsilon) = -H_t(x_0) \frac{(a_0^2\bar{h}^2 + b_0)\text{sign}(\bar{h})}{\sqrt{(a_0\bar{h}^2 + H_t(x_0)b_0)^2 - 4\bar{h}^2b_0}},$$

which simplifies to ρ_0 given by (8).

Step 4: *Linking the reduced map \bar{P}_ε to the full map P_ε . First, we show that the map P_ε has a fixed point h_ε close to the fixed point \bar{h}_ε of the map \bar{P}_ε (still leaving verification of condition (10) of Lemma 1 for later). We will search for h_ε in the form*

$$h_\varepsilon = \bar{h}_\varepsilon + \varepsilon^{3/4}\tau_\varepsilon, \quad (14)$$

where τ_ε is an ε -dependent constant to be determined. Substituting (14) to (12) we get the following equation for τ_ε :

$$\bar{P}_\varepsilon(\bar{h}_\varepsilon + \varepsilon^{3/4}\tau) + o(\bar{h}_\varepsilon + \varepsilon^{3/4}\tau, \varepsilon) = \bar{h}_\varepsilon + \varepsilon^{3/4}\tau.$$

Since $\bar{P}_\varepsilon(\bar{h}_\varepsilon) = \bar{h}_\varepsilon$, we obtain

$$(\bar{P}_\varepsilon)'(\bar{h}_\varepsilon)\varepsilon^{3/4}\tau + I(\varepsilon, \tau)(\varepsilon^{3/4}\tau)^2 + o(\bar{h}_\varepsilon + \varepsilon^{3/4}\tau, \varepsilon) = \varepsilon^{3/4}\tau,$$

and dividing by $\varepsilon^{3/4}$,

$$(\bar{P}_\varepsilon)'(\bar{h}_\varepsilon)\tau + I(\varepsilon, \tau)\varepsilon^{3/4}\tau^2 + \frac{o(\bar{h}_\varepsilon + \varepsilon^{3/4}\tau, \varepsilon)}{\varepsilon^{3/4}} - \tau = 0.$$

Denoting the left-hand-side of the last equation by $F(\tau, \varepsilon)$, we can use the implicit function theorem to solve $F(\tau, \varepsilon) = 0$. Indeed, noticing that (12)-(13) imply that $o(\bar{h}_\varepsilon + \varepsilon^{3/4}\tau, \varepsilon)$ is of order ε , we conclude $F(0, 0) = 0$. To establish $F_\tau(0, 0) \neq 0$ we verify that

$$\frac{d}{d\tau} \left(\frac{o(\bar{h}_\varepsilon + \varepsilon^{3/4}\tau, \varepsilon)}{\varepsilon^{3/4}} \right) = o_h(\bar{h}_\varepsilon + \varepsilon^{3/4}\tau, \varepsilon) \rightarrow 0$$

as $\varepsilon \rightarrow 0$, yielding $F_\tau(0, 0) = \rho_0 - 1 \neq 0$ by (6). From the implicit function theorem we now obtain $\tau_\varepsilon \rightarrow 0$ as $\varepsilon \rightarrow 0$ such that $F(\tau_\varepsilon, \varepsilon) = 0$ for all $\varepsilon \neq 0$ and so (14) holds true.

To show that stability of the fixed point h_ε of P_ε coincides with stability of the fixed point \bar{h}_ε of \bar{P}_ε , we observe that

$$\rho_\varepsilon = (P_\varepsilon)'(h_\varepsilon) \rightarrow (\bar{P}_\varepsilon)'(\bar{h}_\varepsilon) = \rho_0, \quad \text{as } \varepsilon \rightarrow 0,$$

because $o_h(\bar{h}_\varepsilon + \varepsilon^{3/4}\tau_\varepsilon, \varepsilon) \rightarrow 0$ as $\varepsilon \rightarrow 0$. Since (6) implies $\rho_0 \in (-1, 1)$, we conclude that $\rho_\varepsilon \in (-1, 1)$ for $\varepsilon > 0$ sufficiently small.

Step 5: *Verification of condition (10) of Lemma 1.* It is sufficient to show the existence of $\gamma > 0$ such that the second inequality of (10) holds with $(h, \varepsilon) = (h_\varepsilon, \varepsilon)$. We have $\frac{(2a_0h_\varepsilon)^2 - 4b_0\varepsilon}{\sqrt{h_\varepsilon^4 + \varepsilon^2}} =$

$$\begin{aligned} &= 4 \frac{(a_0\bar{h}^2 + H_t(x_0)b_0 + a_0\varepsilon^{1/4}\tau_\varepsilon 2\bar{h})^2 - 4b_0\bar{h}^2}{\sqrt{(\bar{h}^2 + H_t(x_0)^2b_0 + \varepsilon^{1/4}\tau_\varepsilon 2\bar{h})^4 + (2\bar{h})^4}} \geq \\ &\geq 2a_0^2 \frac{(\bar{h}^2 + b_0/a_0^2)^2 - 4b_0\bar{h}^2/a_0^2}{\sqrt{(\bar{h}^2 + H_t(x_0)^2b_0)^4 + (2\bar{h})^4}}, \end{aligned} \quad (15)$$

for all $\varepsilon > 0$ sufficiently small. And strict positivity of (15) follows by assumption (6).

Let now $t \mapsto (v_\varepsilon(t), h_\varepsilon(t))$ be the solution of (1)-(2) with the initial condition $(v_{th} + \varepsilon\bar{v}, h_\varepsilon)$, i.e. $t \mapsto (v_\varepsilon(t), h_\varepsilon(t))$ takes the value $(v_{th} + \varepsilon\bar{v}, h_\varepsilon)$ right after the reset law (2) is applied, that we formulate as $(v_\varepsilon(0^+), h_\varepsilon(0^+)) = (v_{th} + \varepsilon\bar{v}, h_\varepsilon)$. Accordingly $t \mapsto (v_\varepsilon(t), h_\varepsilon(t))$ takes the value $(v_{th}, h_\varepsilon - \sqrt{\varepsilon} \cdot \bar{h})$ right before (2) is applied, that is recorded as $(v_\varepsilon(0^-), h_\varepsilon(0^-)) = (v_{th}, h_\varepsilon - \sqrt{\varepsilon} \cdot \bar{h})$.

Step 6: *Verifying that solution $(v_\varepsilon(t), h_\varepsilon(t))$ with the initial condition $(v_{th} + \varepsilon\bar{v}, h_\varepsilon)$ doesn't cross the firing threshold $v = v_{th}$ on the open interval $(0, T(h_\varepsilon, \varepsilon))$.* From equation (1) we conclude that the set of all points of the vector field of (1)-(2) where $\dot{v} = 0$ is given by

$$h = L(v) \quad \text{with} \quad L(v) = -(\varepsilon m_1 v + \varepsilon m v^2)/k_1.$$

Claim: If $v_\varepsilon(t_\varepsilon) = v_{th}$ for $t_\varepsilon \in (0, T(h_\varepsilon, \varepsilon))$ then $\dot{v}_\varepsilon(s_\varepsilon) = 0$ with $h_\varepsilon(s_\varepsilon) \neq L(v_\varepsilon(s_\varepsilon))$ at some $s_\varepsilon \in (0, t_\varepsilon)$ contradicting definition of the curve L .

Proof of the Claim. Step I. To prove that

$$h_\varepsilon(0^+) < L(v), \quad \text{for all } v \in [0, v_{th}],$$

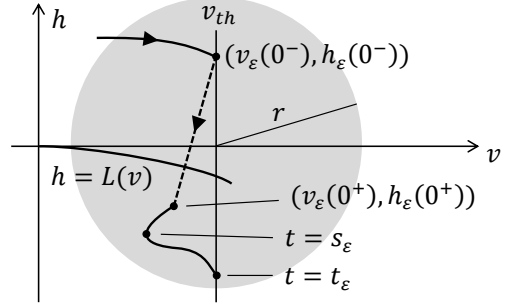


Fig. 4 Illustration of the proof of the claim.

we divide this inequality by $\sqrt{\varepsilon}$ and use (13)-(14) to get the following equivalent inequality

$$\frac{\bar{h}^2 + H_t(x_0)^2b_0}{2\bar{h}} + \varepsilon^{1/4}\tau_\varepsilon + \bar{h} < -\frac{\sqrt{\varepsilon}(m_1v + mv^2)}{k_1},$$

which holds for all $v \in [0, v_{th}]$ by assumption (7), if $\varepsilon > 0$ is sufficiently small.

Step II. Observing from (1) that

$$\frac{\dot{v}_\varepsilon(0^+)}{\sqrt{\varepsilon}} \rightarrow k_1 \left(\frac{\bar{h}^2 + H_t(x_0)^2b_0}{2\bar{h}} + \bar{h} \right) \quad \text{as } \varepsilon \rightarrow 0,$$

we use assumptions (3) and (7) to conclude $\dot{v}_\varepsilon(0^+) < 0$ for all $\varepsilon > 0$ sufficiently small. Therefore, $v_\varepsilon(t_\varepsilon) = v_{th}$ implies the existence of $s_\varepsilon \in (0, t_\varepsilon)$ such that $\dot{v}_\varepsilon(s_\varepsilon) = 0$.

Step III. Now we fix $r \in (0, v_{th})$ and observe that, when $\varepsilon > 0$ is sufficiently small, the vector field (1)-(2) satisfies $\dot{h} < 0$ for any (v, h) from an r -neighborhood of $(v_{th}, 0)$ by assumption (3). Therefore, because $h_\varepsilon(0^+)$ is already below $L([0, v_{th}])$, $h_\varepsilon(s_\varepsilon)$ must be below $L([0, v_{th}])$ as well, i.e. $h_\varepsilon(s_\varepsilon) \neq L(v_\varepsilon(s_\varepsilon))$ and the desired Claim has been achieved.

The proof of the theorem is complete.

Remark 1 One can see from the proof of Theorem 1 (and also by looking at formula (8) for ρ_0) that out of two conditions (6) and (7), condition (6) is responsible for stability of a fixed point of the Poincaré map of system (1)-(2) while condition (7) prohibits repeated impacts of the corresponding periodic cycle (i.e. ensures that exactly 1 spike occurs during 1 period).

2.2 Use of random processes to produce fluctuations in spike threshold

To investigate robustness of qualitative predictions of Theorem 1, we incorporate a random process into the threshold condition of our system as follows:

$$v(t) \rightarrow v(t) + \varepsilon \bar{v}, \quad h(t) \rightarrow h(t) + \sqrt{\varepsilon} \cdot \bar{h}, \quad (16)$$

if $v(t) = v_{th} + \text{noise}(t)$,

with $\text{noise}(t)$ being a Wiener process, which replaces the deterministic reset condition (2). The addition of a Wiener process provides a slowly varying, stochastic noise term to the threshold condition, allowing for realistic variability in the spike threshold of the system.

We are interested to determine how the phase-locking prediction of Theorem 1 (one spike per oscillation) is affected by the noise addition. To do this, we simulate the dynamics of the system of (1) and (16) for a range of the values of v_{th} that satisfy or violate conditions of Theorem 1.

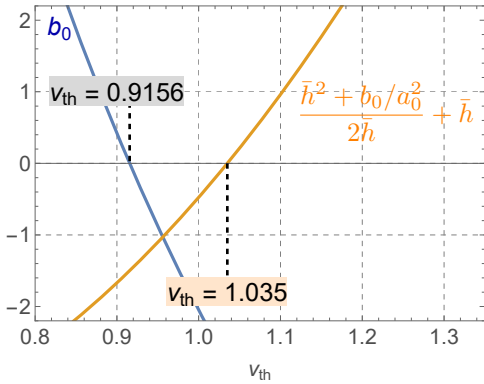


Fig. 5 Graphs of b_0 and $\frac{\bar{h}^2 + b_0/a_0^2}{2\bar{h}} + \bar{h}$ from (6)-(7) as function of v_{th} with other parameters given by (17).

3 Results

3.1 Autonomous case

In this section we pick parameters satisfying Theorem 1 except for v_{th} that we vary in order to demonstrate the agreement of stability prediction (8) with numerical simulations. Specifically,

considering

$$\begin{aligned} k_1 &= 0.18, & k_2 &= -1, & m_1 &= 0.645, \\ m_2 &= -0.35, & m &= 0.3, & \bar{h} &= -1, & \bar{v} &= -2, \end{aligned} \quad (17)$$

we compute the quantities in (6) and (7) as functions of v_{th} . The graphs of these functions are shown in Fig. 5, from where we conclude that, for parameters (17) and focusing on $v_{th} > 0$, conditions (6)-(7) for the existence of an asymptotically stable 1-period discontinuous limit cycle hold when

$$0.9156 < v_{th} < 1.035. \quad (18)$$

By considering a particular value

$$v_{th} = 1,$$

simulations of Fig. 6 document that for $\varepsilon > 0$ sufficiently small the dynamics of (1)-(2) is indeed a cycle of one impact per oscillation.

We then simulate the dynamics of (1)-(2) for increasing values of $\varepsilon > 0$ to examine how violation of the assumption of Theorem 1 about the smallness of $\varepsilon > 0$ manifests itself in qualitative properties of oscillations. We conclude that increase of ε from 0 to $\varepsilon = 0.25$ first increases the number of impacts per period of the discontinuous cycle (i.e. increases the period of the cycle) and then decreases this number (see Figs. 6). We were unable to observe that increasing period is period doubling. Simulations for the values of parameters of ε between cycles of different periods suggest chaotic windows. Indeed, the intervals of ε between the values $\varepsilon = 0.08, \varepsilon = 0.1, \varepsilon = 0.18, \varepsilon = 0.2, \varepsilon = 0.25$ all contain a seemingly chaotic discontinuous cycle as the one shown in Fig. 6 for $\varepsilon = 0.19$.

We recall that according to Remark 1, the left end of the interval (18) is the critical value of parameter v_{th} where the 1-period cycle is supposed to loose stability. Simulation of Fig. 7 shows perfect agreement with this prediction: 1-period cycle transforms to cycle of higher period when v_{th} crosses $v_{th} = 0.9156$ from the right to the left.

Finally, we would like to demonstrate that parameter prediction of Theorem 1 is important for making the spikes of system (1)-(2) to occur at the

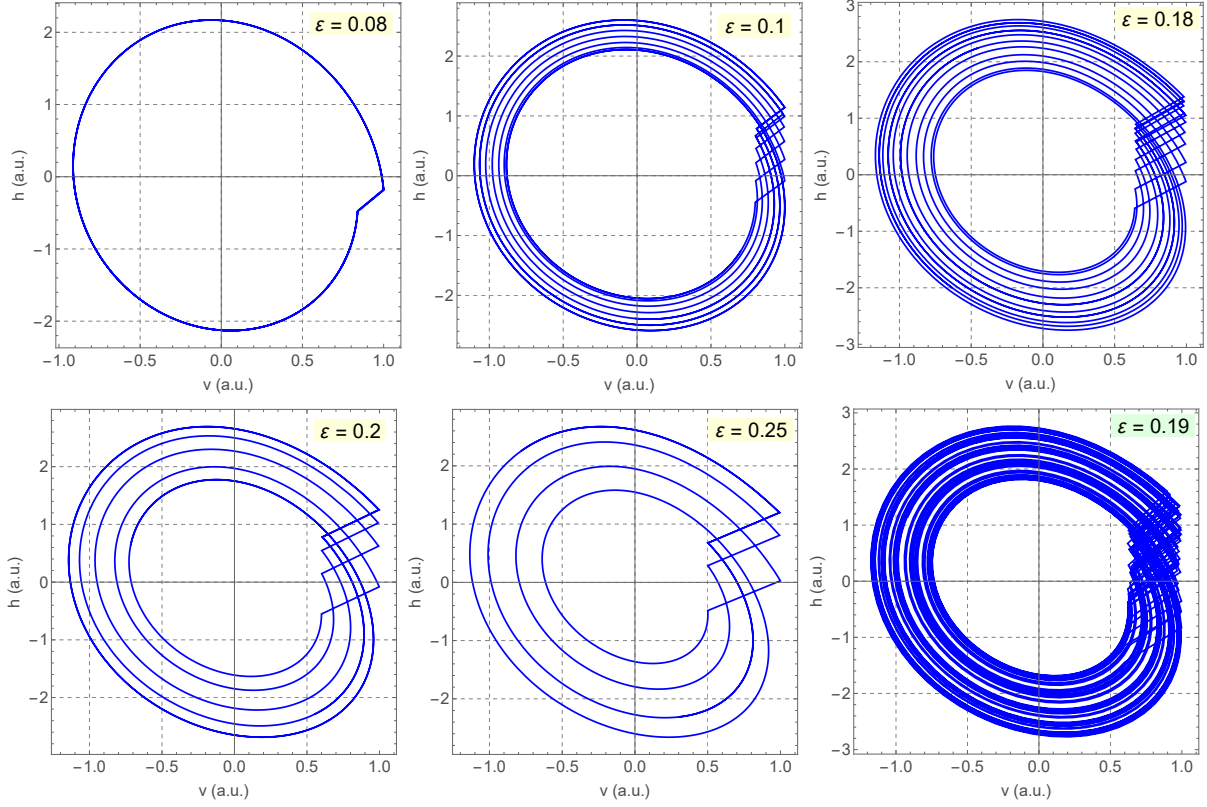


Fig. 6 Simulations of system (1)-(2) for parameters (17), $v_{th} = 1$, and varying ε .

top of membrane potential, rather than to occur on the rising phase of potential. Indeed, in Fig. 8 we violate conditions of Theorem 1 in two different ways (by reducing v_{th} and by increasing ε) and observe that each of the two ways shifts the spikes from the top of membrane potential.

3.1.1 The case of stable focus

Because conditions of Theorem 1 concern the local behavior of system (1)-(2) (near a grazing cycle of (4)), Theorem 1 is capable to design asymptotically stable spiking oscillations not only when the center of (4) transforms to unstable focus of (1), but also in the less intuitive case when the center of (4) transforms to an asymptotically stable focus of (1) (see Fig. 9), meaning that Theorem 1 is capable to design multi-stability.

3.1.2 The case of repeated impacts

Even though condition (7) prevents repeated impacts in the proof of Theorem 1, repeated

impacts are possible when condition (7) is violated, as Fig. 10 documents. Moreover, Fig. 10 suggests that any number of repeated impacts per oscillation (and close to the peak of membrane potential) is possible. Therefore, generalization of Theorem 1 for the case of a desired number of repeated impacts is a feasible project.

3.2 Non-autonomous case

In this section we analyze numeric simulations of the model of (1) with the reset rule (16) and with particular parameters of the Wiener process $noise(t)$ of (16). Specifically, in this section,

$noise(t)$ is a Wiener process with drift 0, (19) volatility 0.5, and scaled by a factor 0.01.

The corresponding Wolfram Mathematica code reads as

```
SeedRandom[seed2use];
sample = RandomFunction[WienerProcess[0, 0.5], {0, timebound, 0.01}];
```

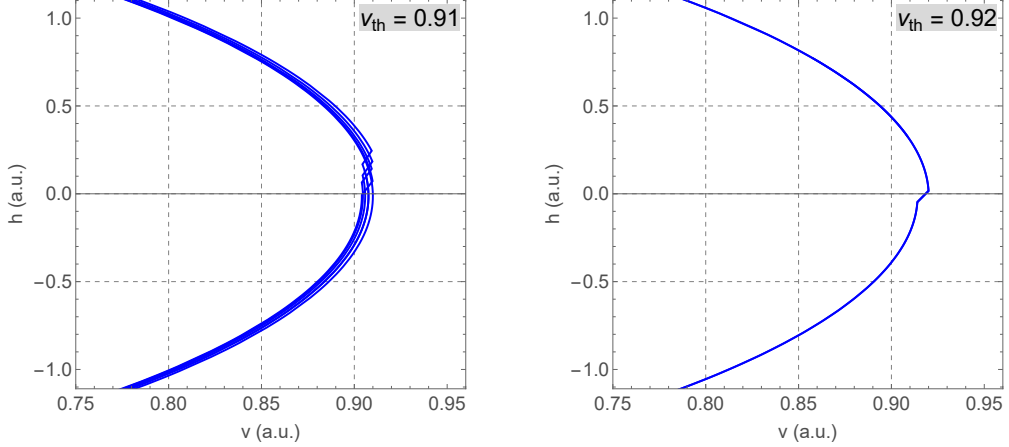


Fig. 7 The attracting solutions of system (1)-(2) with $v_{th} < 0.9156$ and $v_{th} > 0.9156$, $\varepsilon = 0.003$, and other parameters as given by (17). The solutions form limit cycle in both cases, but we zoom a part of limit cycles to make the impact visible.

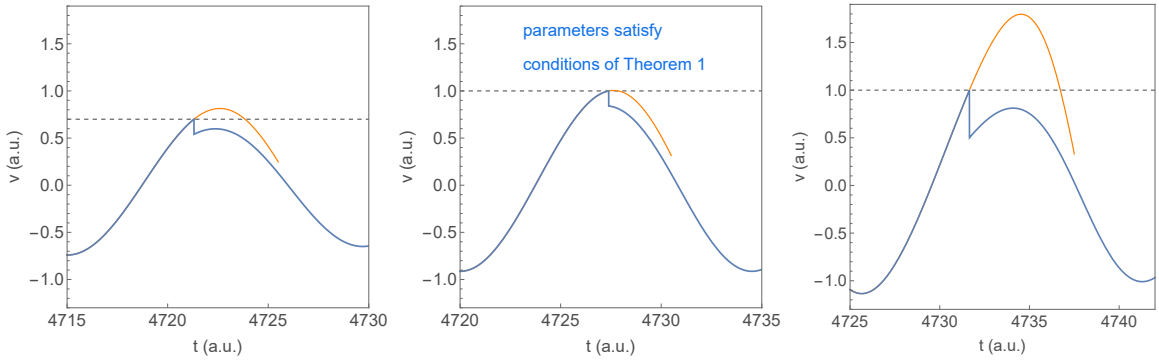


Fig. 8 The membrane potential $v(t)$ is shown as a function of time for the model (1)-(2) with the parameters (17) except for the following: Left: $v_{th} = 0.7$, $\varepsilon = 0.08$, Middle: $v_{th} = 1$, $\varepsilon = 0.08$, Right: $v_{th} = 1$, $\varepsilon = 0.25$.

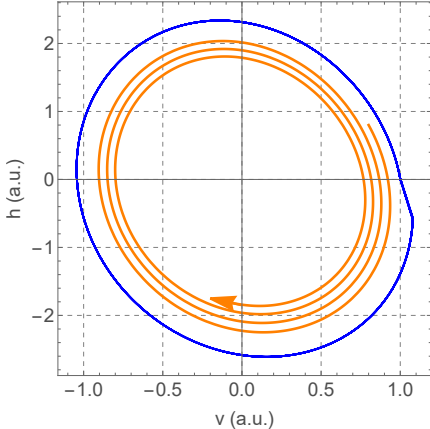


Fig. 9 The attracting solutions of system (1)-(2) with $\varepsilon = 0.08$, $k_1 = 0.18$, $m = 0.3$, $m_1 = 0.645$, $\bar{h} = -1$, $k_2 = -1$, $m_2 = 0.748$, $\bar{v} = 1$, $v_{th} = 1$.

data = TimeSeries[sample, ResamplingMethod

-> "Interpolation", InterpolationOrder -> 1];
 $\text{noise}[t_-] = 0.01*\text{data}["\text{PathFunction}"][[t]]$;

The graph of $\text{noise}(t)$ is shown in Fig. 11 and the location of oscillations of the system of (1) and (16) relative to the location of oscillations of system (1)-(2) is shown in Fig. 12.

From simulations of Fig. 13 we conclude that parameters' prediction of Theorem 1 are remarkably robust. Indeed, noise perturbation has almost no influence on the dynamics predicted by Theorem 1 when parameters of the unperturbed system satisfy the conditions of the theorem (i.e. we do see exactly 1 spike per oscillation in the middle simulation of Fig. 13). Violation of conditions of Theorem 1 for the unperturbed system by varying v_{th} beyond the requirement (18) leads to either smaller number of spikes per oscillation

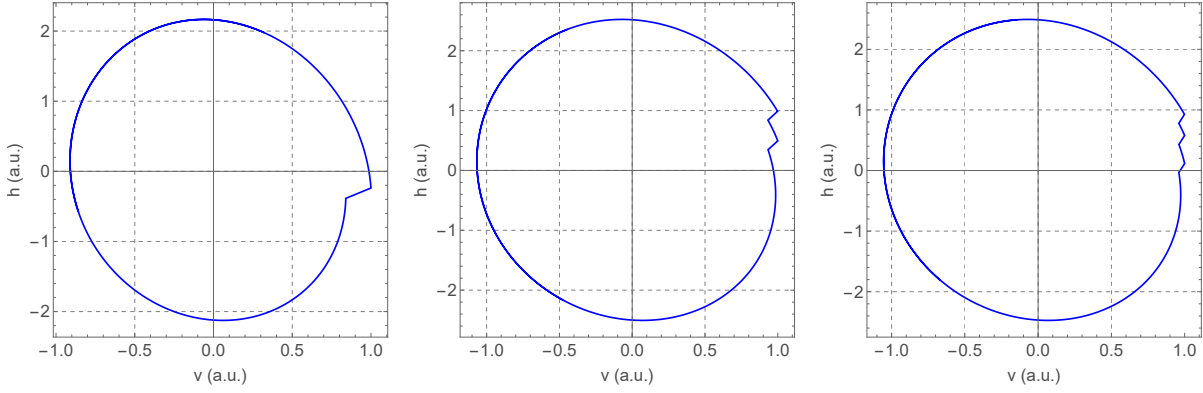


Fig. 10 The attracting solutions of system (1)-(2) with $\varepsilon = 0.08$, $k_1 = 0.18$, $m = 0.3$, $m_1 = 0.645$, $\bar{h} = -0.5$, $k_2 = -1$, $m_2 = -0.35$, $v_{th} = 1$. The value of \bar{v} is varied: Left: $\bar{v} = -2$, Middle: $\bar{v} = -0.85$, Right: $\bar{v} = -0.5$.

(bottom simulation of Fig. 13) or greater number of spikes per oscillation (top simulation of Fig. 13), but the system keeps spiking in either case because the presence of unstable focus keeps widen the trajectory until it reaches the reset threshold.

Overall, we conclude that the graph of v -dynamics of the system of (1) and (16) (Fig. 13) resembles some typical aspects of the dynamics of Fig. 1 of Domnisoru et al. (2013).

Additionally, in Fig. 14 we simulate the system of (1) and (16) for the parameters corresponding to the case of the repeated spiking of Fig. 10(right) to demonstrate that the qualitative properties of the dynamics of Fig. 10 (repeated spiking close to the peak of membrane potential) are robust with respect to noise perturbation, meaning that developing an analogue of Theorem 1 for the case of repeated spiking promises to be a successful project that will provide further analytic support to the dynamics of Fig. 1 of Domnisoru et al. (2013).

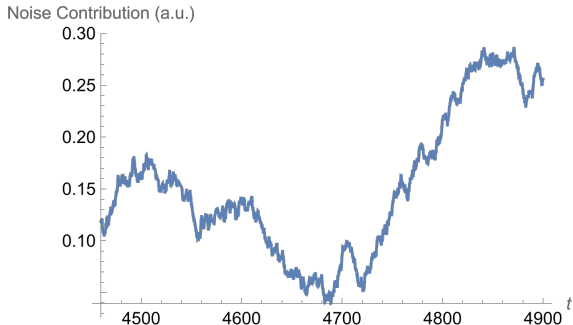


Fig. 11 The graph of Wiener process $noise(t)$ as defined in (19).

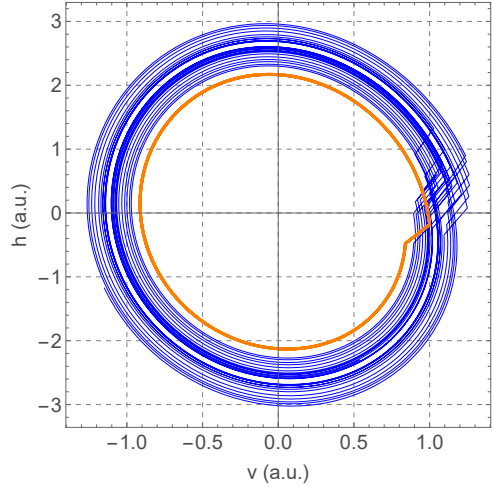


Fig. 12 The limit cycle of model (1)-(2) (the closed orange curve) with parameters given by (17), and $v_{th} = 1$, $\varepsilon = 0.08$ and the corresponding solution of the system of (1) and (16) (the black trajectory with multiple resets). The black (outer) trajectory cycles in a clockwise direction, resetting when it crosses the (moving) threshold.

4 Discussion

The model presented here demonstrates how individual neurons could maintain spiking that is phase locked to the peak or right before the peak of intracellular membrane potential oscillations. An important component of this process is a model with an unstable center, resulting in a neuron that shows progressively larger oscillations that spiral out from the center until reaching the spiking threshold. The reset of membrane potential after each spiking event results in a limit cycle that continues to graze the threshold on subsequent cycles, resulting in spikes that occur near

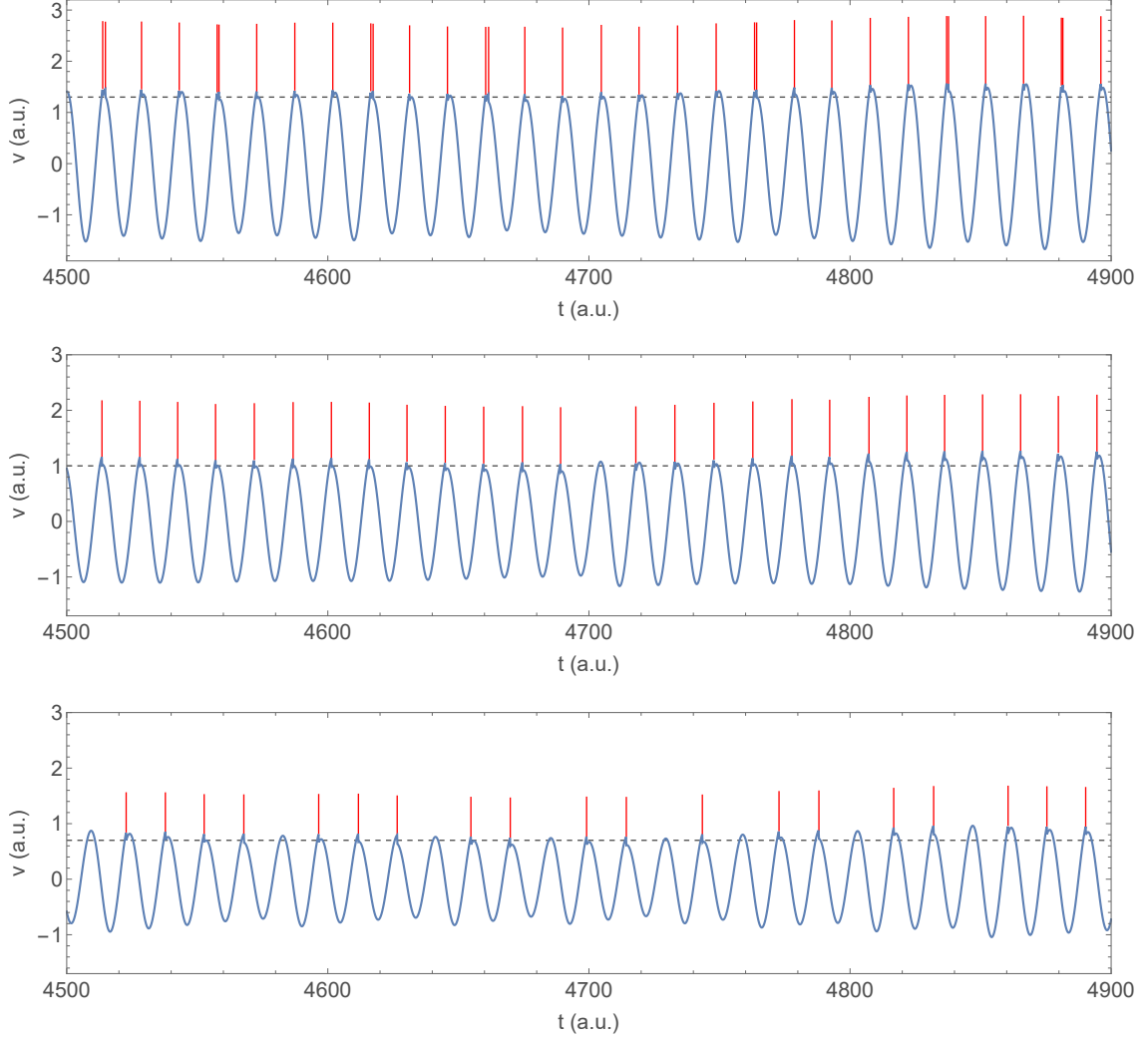


Fig. 13 The membrane potential $v(t)$ is shown as a function of time for the model (1) with noise added to the reset threshold according to (16). The parameters are set as (17) and (19). The value of ε is $\varepsilon = 0.08$ and v_{th} is taken as $v_{th} = 1.3$ (top figure), $v_{th} = 1$ (middle figure), $v_{th} = 0.7$ (bottom figure). The values of v_{th} is represented by the horizontal dashed lines. Note, the actual reset value is not v_{th} , but v_{th} with noise added according to (16) and (19). The spikes were added manually at each reset (in red).

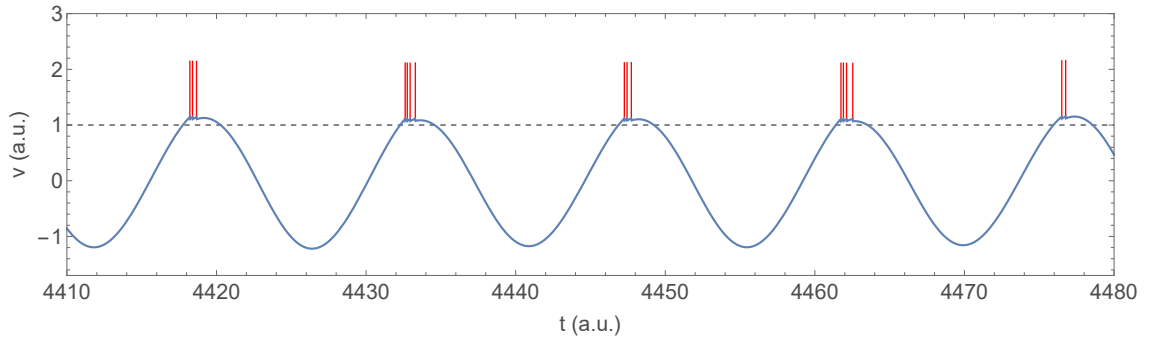


Fig. 14 The membrane potential $v(t)$ as in Fig. 13 except for parameters changed as follows: $\bar{h} = -0.5$, $\bar{v} = -0.5$, $v_{th} = 1$.

the peak of a cycle. Biologically, an unstable center could be provided by intrinsic ionic mechanisms such as those that support spontaneous subthreshold theta oscillations (Bal and McCormick 1997; Boehmer et al. 2000).

As shown in Figures 12 and 13, this model provides a potential mechanism for the experimental observation of spikes occurring near the peak of each oscillation of membrane potential (Harvey et al. 2009; Domnisoru et al. 2013; Schmidt-Hieber and Häusser 2013). Incorporating a variable threshold as seen biologically (Higgs and Spain 2011; Platkiewicz and Brette 2011; Tsuno et al. 2013; Wester and Contreras 2013; Fontaine et al. 2014) allows the model to replicate the data in which the membrane potential and spiking onset vary across oscillation cycles, resulting in the appearance of spikes at different membrane potentials (Domnisoru et al. 2013).

This mechanism for maintaining spiking at the peak of each oscillation could be relevant to oscillatory interference models of theta phase precession that require spikes to occur near the peak of each cycle, as required in models of theta phase precession which utilize an intrinsic oscillation that maintains intrinsic spiking at one phase relative to the network oscillation (O'Keefe and Recce 1993; Lengyel et al. 2003; Burgess et al. 2007; Bush and Burgess 2014; Hasselmo and Shay 2014; Hasselmo 2014). It should be noted that oscillatory interference is only one potential model of theta phase precession, as precession has also been attributed to different mechanisms including read out of sequences or the influence of an asymmetrical ramp of depolarization that interacts with oscillatory input to cause spikes to advance to earlier phases with greater depolarization (Kamondi et al. 1998; Mehta et al. 2002).

The maintenance of spiking at a specific phase of intracellular oscillations, coupled with the shift in phase of oscillations relative to network field potential could contribute to the encoding and retrieval of memories. Different phases of hippocampal theta show different functional dynamics that are proposed to underlie separate phases of encoding and retrieval (Hasselmo et al. 2002). The role of different phases is supported by neurons showing differential phase of firing for novel stimuli versus familiar stimuli (Zilli and Hasselmo 2006; Manns et al. 2007; Lever et al. 2010), by EEG traces in human performing memory

tasks (Rizzuto et al. 2006; Kerrén et al. 2018), and by the correlation between theta phase and eye fixations on novel versus retrieved locations (Kragel et al. 2020). Additionally, the inhibition of hippocampal neurons causes selective effects on behavior depending on the phase of the manipulation (Siegle and Wilson 2014).

To produce this neuron model that maintains a spiking phase preference relative to the intracellular theta oscillation, we began with a simple linear model that resembles the nonlinear Izhikevich neuron model for resonate-and-fire neurons with some key differences. The inclusion of a small parameter ϵ introduced an unstable focus to the system. The unstable focus of our model cell differs from Izhikevich models, which generally employ a stable resting potential or an oscillating potential that dampens with time. However, there is experimental evidence for sustained subthreshold oscillations and other spontaneous intrinsic activity *in vivo* (Bal and McCormick 1997; Boehmer et al. 2000; Häusser et al. 2004).

Additionally, the spiking threshold of our model varied over time. Variability in spike threshold, as seen biologically (Higgs and Spain 2011; Platkiewicz and Brette 2011; Tsuno et al. 2013; Wester and Contreras 2013; Fontaine et al. 2014), is not often implemented in spiking cell models. However, the unstable focus in the membrane potential of our model enabled the cell to reliably reach the variable spiking threshold. Biologically, the parameter ϵ may be interpreted as a contribution of multiple ion channel types to the neuron. The membrane potential dynamics are likely to incorporate both an afterhyperpolarizing potassium current (in the reset equation) and a depolarizing mixed cation current (in the voltage equation).

Models of the cellular contributions to spatial processing in brain networks continue to play a significant role in advancing our ideas of how the brain produces spatial cognition. The equations of our model cell are straightforward to implement and have the benefit of modeling a cell that can fire near the peak of the theta rhythm even on theta cycles where the baseline potential was relatively depolarized, similar to dynamics observed *in vivo* (Dominisoru et al. 2013). We hope these equations can be of use to modelers and others in the study of spatial processing.

Acknowledgments

This collaboration was made possible by the Burroughs Wellcome Fund with a Collaborative Research Travel Grant #1017453 to OM to visit MH at the Center for Systems Neuroscience at Boston University. OM thanks the Center for providing excellent working conditions. This work was also supported by the National Institutes of Health and the Office of Naval Research. The authors are grateful to anonymous reviewers for useful comments that helped to improve the quality of the paper.

Declarations

- Conflict of interest/Competing interests. The author declares no competing interests.

Appendix A Proofs of lemmas

Proof of Lemma 1. By expressing (ε, h^2) in polar coordinates (for $r > 0, \phi \in [0, 2\pi] \setminus \{0, 2\pi\}$),

$$\varepsilon = r \sin \phi, \quad h^2 \operatorname{sign}(h) = r \cos \phi,$$

i.e. 0 and 2π are identified, we observe that equation (9) can be rewritten as

$$\begin{aligned} & t^2 + at\sqrt{r|\cos \phi|} \cdot \alpha + br \sin \phi + ctr \sin \phi + \\ & + p\sqrt{r|\cos \phi|}r \sin \phi \cdot \alpha + qr^2 \sin^2 \phi + \\ & + I(t, r, \phi) \left(\frac{t}{r \sin \phi} \right)^3 = 0, \quad \alpha = \operatorname{sign}(h) \end{aligned}$$

which contains just one small parameter $r > 0$ as opposed to the two small parameters $\varepsilon > 0$ and $h > 0$ in the initial equation (9). Moreover, the equation obtained suggests that $t \sim \sqrt{r}$, which hints at searching for t in the form

$$t = \sqrt{rs}.$$

This change of the variable yields, upon dividing by r ,

$$\begin{aligned} & s^2 + as\sqrt{|\cos \phi|} \cdot \alpha + b \sin \phi + c\sqrt{rs} \sin \phi + \\ & + p\sqrt{r|\cos \phi|} \sin \phi \cdot \alpha + qr \sin \phi + J(s, r, \phi) = 0, \end{aligned} \tag{A1}$$

where

$$J(s, r, \phi) = \frac{I(s, r, \phi)}{r} \left(\begin{array}{c} \sqrt{rs} \\ \sqrt{r|\cos \phi|} \cdot \alpha \\ r \sin \phi \end{array} \right)^3 = \sqrt{r} I(s, r, \phi) \left(\begin{array}{c} s \\ \sqrt{|\cos \phi|} \cdot \alpha \\ \sqrt{r} \sin \phi \end{array} \right)^3.$$

Denoting the left hand side of (A1) by $F(s, \sqrt{r}, \phi)$, we observe that the two solutions s of $F(s, 0, \phi) = 0$ are given by

$$s_{\pm}(\phi) = \frac{1}{2} \left(-a\sqrt{|\cos \phi|} \cdot \alpha \pm \sqrt{a^2|\cos \phi| - 4b \sin \phi} \right),$$

provided that $a^2|\cos \phi| - 4b \sin \phi > 0$. Moreover, $F_s(s_{\pm}(\phi), 0, \phi) = 2s_{\pm}(\phi) + a\sqrt{|\cos \phi|} \cdot \alpha = \pm\sqrt{a^2|\cos \phi| - 4b \sin \phi} = \pm\frac{(ah)^2 - 4b\varepsilon}{\sqrt{h^4 + \varepsilon^2}}$. Therefore, by the implicit function theorem (that applies thanks to condition (10)), given $\gamma > 0$ there exists $\delta > 0$ such that for any $r \in [0, \delta]$ and for any $\phi \in [0, 2\pi]/\{0, 2\pi\}$ such that $a^2|\cos \phi| - 4b \sin \phi \geq \gamma$, the equation $F(s, \sqrt{r}, \phi) = 0$ has two solutions: a unique solution $S(\sqrt{r}, \phi) \rightarrow s_-(\phi)$ as $r \rightarrow 0$ and a unique solution approaching $s_+(\phi)$ as $r \rightarrow \infty$. Since $s_-(\phi) < s_+(\phi)$ (i.e. $s_-(\phi)$ is the least solution) it remains to show that $S(\sqrt{r}, \phi)$ matches the formula that the lemma claims. By the implicit function theorem, the solution $(\sqrt{r}, \phi) \rightarrow S(\sqrt{r}, \phi)$ is C^2 in the above-defined domain of definition, see e.g. (Zorich 2004, §8.5.4, Theorem 1). Therefore $S(\sqrt{r}, \phi)$ can be expanded in Taylor series as follows

$$\begin{aligned} S(\sqrt{r}, \phi) &= S(0, \phi) + I(\sqrt{r}, \phi)\sqrt{r} = \\ &= \frac{1}{2} \left(-a\sqrt{|\cos \phi|} \cdot \alpha - \sqrt{a^2|\cos \phi| - 4b \sin \phi} \right) + \\ &\quad + I(\sqrt{r}, \phi)\sqrt{r}, \end{aligned}$$

where I is C^1 smooth on $r \in [0, \delta]$, $\phi \in [0, 2\pi]/\{0, 2\pi\}$, and $I_{\phi}(0, 0^+) = I_{\phi}(0, 2\pi^-)$. Returning back to the variable t , we get

$$\begin{aligned} t &= \sqrt{r}S(\sqrt{r}, \phi) = \frac{1}{2} \left(-ah - \sqrt{(ah)^2 - 4b\varepsilon} \right) + \\ &\quad + I(h, \varepsilon)\sqrt{h^4 + \varepsilon^2}, \end{aligned} \tag{A2}$$

where I is C^1 -smooth on $\sqrt{h^4 + \varepsilon^2} \leq \delta$. The proof of the lemma is complete.

Proof of Lemma 2. By solving the linear system (4), one gets

$$\begin{aligned} \begin{pmatrix} V(t, v, h, 0) \\ H(t, v, h, 0) \end{pmatrix} &= \Omega(t) \begin{pmatrix} v \\ h \end{pmatrix}, \\ \Omega(t) &= \begin{pmatrix} \cos(\omega t) & (k_1/\omega) \sin(\omega t) \\ (k_2/\omega) \sin(\omega t) & \cos(\omega t) \end{pmatrix}. \end{aligned} \tag{A3}$$

In particular, $\Omega(T_0) = I$, $\Omega'(T_0) = \begin{pmatrix} 0 & k_1 \\ k_2 & 0 \end{pmatrix}$, $\Omega''(T_0) = \begin{pmatrix} -\omega^2 & 0 \\ 0 & -\omega \end{pmatrix}$, $V(x_0) = v_{th}$, $H(x_0) = 0$. Thus, (A3) implies

$$\begin{aligned} V_v(x_0) &= H_h(x_0) = 1, \quad V_h(x_0) = H_v(x_0) = 0, \\ V_t(x_0) &= k_1 H(x_0) = 0, \\ H_t(x_0) &= k_2 V(x_0) = k_2 v_{th}, \\ V_{th}(x_0) &= k_1, \quad V_{tt}(x_0) = -\omega^2 v_{th}. \end{aligned}$$

Since $V(t, v, h, 0)$ and $H(t, v, h, 0)$ are linear in (v, h) , we get that all second-order partial derivatives of V and H with respect to v and h (including second-order mixed partial derivatives) equal 0.

To compute the derivative $(V_{\varepsilon}, H_{\varepsilon})$ we differentiate (1) with respect to ε obtaining a linear inhomogeneous system

$$\dot{y} = \begin{pmatrix} 0 & k_1 \\ k_2 & 0 \end{pmatrix} y + f(t), \tag{A4}$$

where

$$\begin{aligned} y &= \begin{pmatrix} V_{\varepsilon}(t, v_{th}, 0, 0) \\ H_{\varepsilon}(t, v_{th}, 0, 0) \end{pmatrix}, \\ f(t) &= \begin{pmatrix} mV(t, v_{th}, 0, 0)^2 + m_1 V(t, v_{th}, 0, 0) \\ m_2 H(t, v_{th}, 0, 0) \end{pmatrix}. \end{aligned}$$

In particular, we have $(V_{\varepsilon}(x_0), H_{\varepsilon}(x_0))^T = y(T_0)$. Noticing that $y(0) = 0$, the variation of constants formula yields

$$y(t) = \Omega(t) \int_0^t \Omega(-s) f(s) ds, \tag{A5}$$

whose full computation is provided in formula (A6). The required formula for $(V_{\varepsilon}(x_0), H_{\varepsilon}(x_0))$ follows by plugging $t = T_0 = 2\pi/\omega$ in formula (A6).

The proof of the lemma is complete.

$$y(t) = \begin{pmatrix} \cos(\omega t) \left(\frac{2m v_{th}^2 \sin(\omega t)}{3\omega} + \frac{tv_{th}(m_1 + m_2)}{2} \right) + v_{th} \sin(t\omega) \frac{2m v_{th} + 3(m_1 - m_2)}{6\omega} \\ \frac{m v_{th}^2 \cos(\omega t)}{3k_1} - \frac{m v_{th}^2 \sin^2(\omega t)}{3k_1} - \frac{t v_{th}(m_1 + m_2)\omega \sin(\omega t)}{2k_1} - \frac{m v_{th}^2}{3k_1} \end{pmatrix} \quad (A6)$$

References

Bal T, McCormick DA (1997) Synchronized Oscillations in the Inferior Olive Are Controlled by the Hyperpolarization-Activated Cation Current I_h . *Journal of Neurophysiology* 77(6):3145–3156. <https://doi.org/10.1152/jn.1997.77.6.3145>

Berry S, Thompson R (1978) Prediction of learning rate from the hippocampal electroencephalogram. *Science* 200(4347):1298–1300. <https://doi.org/10.1126/science.663612>

Boehmer G, Greffrath W, Martin E, et al (2000) Subthreshold oscillation of the membrane potential in magnocellular neurones of the rat supraoptic nucleus. *The Journal of Physiology* 526(1):115–128. <https://doi.org/10.1111/j.1469-7793.2000.t01-1-00115.x>

Burgess N, Barry C, O’Keefe J (2007) An oscillatory interference model of grid cell firing. *Hippocampus* 17(9):801–812. <https://doi.org/10.1002/hipo.20327>

Bush D, Burgess N (2014) A Hybrid Oscillatory Interference/Continuous Attractor Network Model of Grid Cell Firing. *The Journal of Neuroscience* 34(14):5065–5079. <https://doi.org/10.1523/jneurosci.4017-13.2014>

Buzsáki G, S. LLW, Vanderwolf CH (1983) Cellular bases of hippocampal EEG in the behaving rat. *Brain Research Reviews* 6(2):139–171. [https://doi.org/10.1016/0165-0173\(83\)90037-1](https://doi.org/10.1016/0165-0173(83)90037-1)

Christopher C, Li C, Torregrosa J (2024) Limit cycles of differential equations, 2nd edn. Advanced Courses in Mathematics. CRM Barcelona, Birkhäuser/Springer, Cham

Coombes S, Thul R, Wedgwood KCA (2012) Nonsmooth dynamics in spiking neuron models. *Phys D* 241(22):2042–2057. <https://doi.org/10.1016/j.physd.2011.05.012>

DiBernardo M, Budd CJ, Champneys AR, et al (2008) Piecewise-smooth Dynamical Systems: Theory and Applications, Applied Mathematical Sciences-Series, vol 163. <https://doi.org/10.1007/978-1-84628-708-4>

Domnisoru C, Kinkhabwala AA, Tank DW (2013) Membrane potential dynamics of grid cells. *Nature* 495(7440):199–204. <https://doi.org/10.1038/nature11973>

Fernández-Ruiz A, Oliva A, Nagy GA, et al (2017) Entorhinal-CA3 Dual-Input Control of Spike Timing in the Hippocampus by Theta-Gamma Coupling. *Neuron* 93(5):1213–1226.e5. <https://doi.org/10.1016/j.neuron.2017.02.017>

Fontaine B, Peña JL, Brette R (2014) Spike-Threshold Adaptation Predicted by Membrane Potential Dynamics In Vivo. *PLoS Computational Biology* 10(4):e1003560. <https://doi.org/10.1371/journal.pcbi.1003560>

Fox SE, Wolfson S, Ranck JB (1986) Hippocampal theta rhythm and the firing of neurons in walking and urethane anesthetized rats. *Experimental Brain Research* 62(3):495–508. <https://doi.org/10.1007/bf00236028>

Fujita Y, Sato T (1964) Intracellular records from hippocampal pyramidal cells in rabbit during theta rhythm activity. *Journal of Neurophysiology* 27(6):1011–1025. <https://doi.org/10.1152/jn.1964.27.6.1011>

Givens BS, Olton DS (1990) Cholinergic and GABAergic Modulation of Medial Septal Area: Effect on Working Memory. *Behavioral Neuroscience* 104(6):849–855. <https://doi.org/10.1037/0735-7044.104.6.849>

Hafting T, Fyhn M, Bonnevie T, et al (2008) Hippocampus-independent phase precession in entorhinal grid cells. *Nature* 453(7199):1248–1252. <https://doi.org/10.1038/nature06957>

Harvey CD, Collman F, Dombeck DA, et al (2009) Intracellular dynamics of hippocampal place cells during virtual navigation. *Nature* 461(7266):941–946. <https://doi.org/10.1038/nature08499>

Hasselmo ME (2014) Neuronal rebound spiking, resonance frequency and theta cycle skipping may contribute to grid cell firing in medial entorhinal cortex. *Philosophical Transactions of the Royal Society B: Biological Sciences* 369(1635):20120523. <https://doi.org/10.1098/rstb.2012.0523>

Hasselmo ME, Shay CF (2014) Grid cell firing patterns may arise from feedback interaction between intrinsic rebound spiking and transverse traveling waves with multiple heading angles. *Frontiers in Systems Neuroscience* 8:201. <https://doi.org/10.3389/fnsys.2014.00201>

Hasselmo ME, Bodelon C, Wyble BP (2002) A Proposed Function for Hippocampal Theta Rhythm: Separate Phases of Encoding and Retrieval Enhance Reversal of Prior Learning. *Neural Computation* 14(4):793–817. <https://doi.org/10.1162/089976602317318965>

Higgs MH, Spain WJ (2011) Kv1 channels control spike threshold dynamics and spike timing in cortical pyramidal neurones. *The Journal of Physiology* 589(21):5125–5142. <https://doi.org/10.1113/jphysiol.2011.216721>

Huang C, Resnik A, Celikel T, et al (2016) Adaptive Spike Threshold Enables Robust and Temporally Precise Neuronal Encoding. *PLOS Computational Biology* 12(6):e1004984. <https://doi.org/10.1371/journal.pcbi.1004984>

Huxter J, Burgess N, O’Keefe J (2003) Independent rate and temporal coding in hippocampal pyramidal cells. *Nature* 425(6960):828–832. <https://doi.org/10.1038/nature02058>

Häusser M, Raman IM, Otis T, et al (2004) The Beat Goes On: Spontaneous Firing in Mammalian Neuronal Microcircuits. *The Journal of Neuroscience* 24(42):9215–9219. <https://doi.org/10.1523/jneurosci.3375-04.2004>

Itskov V, Curto C, Pastalkova E, et al (2011) Cell Assembly Sequences Arising from Spike Threshold Adaptation Keep Track of Time in the Hippocampus. *The Journal of Neuroscience* 31(8):2828–2834. <https://doi.org/10.1523/jneurosci.3773-10.2011>

Izhikevich EM (2001) Resonate-and-fire neurons. *Neural Networks* 14(6-7, SI):883–894. [https://doi.org/10.1016/S0893-6080\(01\)00078-8](https://doi.org/10.1016/S0893-6080(01)00078-8)

Izhikevich EM (2007) Dynamical systems in neuroscience: the geometry of excitability and bursting. *Computational Neuroscience*, MIT Press, Cambridge, MA

Kamondi A, Acsády L, Wang X, et al (1998) Theta oscillations in somata and dendrites of hippocampal pyramidal cells in vivo: Activity-dependent phase-precession of action potentials. *Hippocampus* 8(3):244–261. [https://doi.org/10.1002/\(sici\)1098-1063\(1998\)8:3<244::aid-hipo7>3.0.co;2-j](https://doi.org/10.1002/(sici)1098-1063(1998)8:3<244::aid-hipo7>3.0.co;2-j)

Kerrén C, Linde-Domingo J, Hanslmayr S, et al (2018) An Optimal Oscillatory Phase for Pattern Reactivation during Memory Retrieval. *Current Biology* 28(21):3383–3392.e6. <https://doi.org/10.1016/j.cub.2018.08.065>

Kragel JE, VanHaerents S, Templer JW, et al (2020) Hippocampal theta coordinates memory processing during visual exploration. *eLife* 9:e52108. <https://doi.org/10.7554/elife.52108>

Lang S (1993) Real and functional analysis, Graduate Texts in Mathematics, vol 142, 3rd edn. Springer-Verlag, New York, <https://doi.org/10.1007/978-1-4612-0897-6>, URL <https://doi.org/10.1007/978-1-4612-0897-6>

Lengyel M, Szatmáry Z, Érdi P (2003) Dynamically detuned oscillations account for the coupled rate and temporal code of place cell firing. *Hippocampus* 13(6):700–714. <https://doi.org/10.1002/hipo.10116>

Leung LWS, Yim CY (1986) Intracellular records of theta rhythm in hippocampal CA1 cells of the rat. *Brain Research* 367(1-2):323–327. [https://doi.org/10.1016/0006-8993\(86\)91611-2](https://doi.org/10.1016/0006-8993(86)91611-2)

Lever C, Burton S, Jeewajee A, et al (2010) Environmental novelty elicits a later theta phase of firing in CA1 but not subiculum. *Hippocampus* 20(2):229–234. <https://doi.org/10.1002/hipo.20671>

Makarenkov O, Lamb JSW (2012) Dynamics and bifurcations of nonsmooth systems: a survey. *Phys D* 241(22):1826–1844. <https://doi.org/10.1016/j.physd.2012.08.002>, URL <https://doi.org/10.1016/j.physd.2012.08.002>

Manns JR, Zilli EA, Ong KC, et al (2007) Hippocampal CA1 spiking during encoding and retrieval: Relation to theta phase. *Neurobiology of Learning and Memory* 87(1):9–20. <https://doi.org/10.1016/j.nlm.2006.05.007>

Marangio L, Galatolo S, Fronzoni L, et al (2019) Phase-locking patterns in a resonate and fire neural model with periodic drive. *BioSystems* 184. <https://doi.org/10.1016/j.biosystems.2019.103992>

Mehta MR, Lee AK, Wilson MA (2002) Role of experience and oscillations in transforming a rate code into a temporal code. *Nature* 417(6890):741–746. <https://doi.org/10.1038/nature00807>

Mukhopadhyay H (2010) The resonate-and-fire neuron: Time dependent and frequency selective neurons in neural networks. URL https://digitalcommons.bucknell.edu/masters_theses/23, master's Thesis

Nicola W, Campbell SA (2016) Nonsmooth bifurcations of mean field systems of two-dimensional integrate and fire neurons. *SIAM J Appl Dyn Syst* 15(1):391–439. <https://doi.org/10.1137/140985846>, URL <https://doi.org/10.1137/140985846>

O'Keefe J, Burgess N (2005) Dual phase and rate coding in hippocampal place cells: Theoretical significance and relationship to entorhinal grid cells. *Hippocampus* 15(7):853–866. <https://doi.org/10.1002/hipo.20115>

O'Keefe J, Recce ML (1993) Phase relationship between hippocampal place units and the EEG theta rhythm. *Hippocampus* 3(3):317–330. <https://doi.org/10.1002/hipo.450030307>

Platkiewicz J, Brette R (2011) Impact of Fast Sodium Channel Inactivation on Spike Threshold Dynamics and Synaptic Integration. *PLoS Computational Biology* 7(5):e1001129. <https://doi.org/10.1371/journal.pcbi.1001129>

Rizzuto DS, Madsen JR, Bromfield EB, et al (2006) Human neocortical oscillations exhibit theta phase differences between encoding and retrieval. *NeuroImage* 31(3):1352–1358. <https://doi.org/10.1016/j.neuroimage.2006.01.009>

Schmidt-Hieber C, Häusser M (2013) Cellular mechanisms of spatial navigation in the medial entorhinal cortex. *Nature Neuroscience* 16(3):325–331. <https://doi.org/10.1038/nn.3340>

Siegle JH, Wilson MA (2014) Enhancement of encoding and retrieval functions through theta phase-specific manipulation of hippocampus. *eLife* 3:e03061. <https://doi.org/10.7554/elife.03061>

Skaggs WE, McNaughton BL, Wilson MA, et al (1996) Theta phase precession in hippocampal neuronal populations and the compression of temporal sequences. *Hippocampus* 6(2):149–172. [https://doi.org/10.1002/\(sici\)1098-1063\(1996\)6:2<149::aid-hipo6>3.0.co;2-k](https://doi.org/10.1002/(sici)1098-1063(1996)6:2<149::aid-hipo6>3.0.co;2-k)

Tsuno Y, Schultheiss NW, Hasselmo ME (2013) In vivo cholinergic modulation of the cellular properties of medial entorhinal cortex neurons. *The Journal of Physiology* 591(10):2611–2627. <https://doi.org/10.1113/jphysiol.2012.250431>

Turaev D, Rom-Kedar V (1998) Elliptic islands appearing in near-ergodic flows. *Nonlinearity* 11(3):575–600. <https://doi.org/10.1088/0951-7715/11/3/010>, URL <https://doi.org/10.1088/0951-7715/11/3/010>

Wester JC, Contreras D (2013) Biophysical mechanism of spike threshold dependence on the

rate of rise of the membrane potential by sodium channel inactivation or subthreshold axonal potassium current. *Journal of Computational Neuroscience* 35(1):1–17. <https://doi.org/10.1007/s10827-012-0436-2>

Winson J (1978) Loss of hippocampal theta rhythm results in spatial memory deficit in the rat. *Science* 201(4351):160–163. <https://doi.org/10.1126/science.663646>

Yagasaki K (2004) Nonlinear dynamics of vibrating microcantilevers in tapping-mode atomic force microscopy. *PHYSICAL REVIEW B* 70(24). <https://doi.org/10.1103/PhysRevB.70.245419>

Zhao X, Dankowicz H (2006) Unfolding degenerate grazing dynamics in impact actuators. *Nonlinearity* 19(2):399–418. <https://doi.org/10.1088/0951-7715/19/2/009>, URL <https://doi.org/10.1088/0951-7715/19/2/009>

Zilli EA, Hasselmo ME (2006) An analysis of the mean theta phase of population activity in a model of hippocampal region CA1. *Network: Computation in Neural Systems* 17(3):277–297. <https://doi.org/10.1080/09548980601028908>

Zorich V (2004) Mathematical analysis. I. Universitext, Springer-Verlag, Berlin